Resistive Switching Characteristics of Tm_2O_3, Yb_2O_3, and Lu_2O_3-Based Metal–Insulator–Metal Memory Devices

Tung-Ming Pan, Chih-Hung Lu, Somnath Mondal, and Fu-Hsiang Ko

***Abstract*—In this paper, we investigated the electroforming-free resistive switching (RS) behavior in the Ru/RE_2O_3/TaN (rare-earth, RE, RE = Tm, Yb, and Lu) memory device fabricated with full room temperature process. The conduction mechanism of RE_2O_3-based memory devices in the low-resistance state is ohmic emission, whereas Tm_2O_3, Yb_2O_3, and Lu_2O_3 memory devices in the high-resistance state are space charge limited conduction (SCLC), ohmic behavior, and SCLC, respectively. The Ru/Lu_2O_3/TaN device showed a high-resistance ratio of $\sim 10^4$, a high device yield of $\sim$70%, a good data retention as long as 10^5 s measured at 85 °C, and a reliable endurance for up to 100 cycles, suggesting the optimal chemical defects (metallic Lu and nonlattice oxygen ion) in Lu_2O_3 film. All of these results suggest that Ru/Lu_2O_3/TaN structure memory is a good candidate for future nonvolatile RS memory applications.**

***Index Terms*—Lu_2O_3, rare-earth (RE), resistive switching (RS), Tm_2O_3, Yb_2O_3.**

I. Introduction

THE resistance memory switching effects of metal oxide materials have recently attracted a great deal of scientific and technological research related to next-generation nonvolatile memory applications in which resistance can be repeatedly switched by an applied voltage [1]. The resistive switching (RS) behavior has been reported in binary metal oxide films, including TiO_2, NiO_x, CoO_x, WO_x, Al_2O_3, HfO_x, and ZrO_2 [2]–[8]. The origin of the RS mechanism is the formation of a conducting path composed of defects, such as metal ions and oxygen vacancies, which is formed and ruptured by applying an external bias [9]. The electroforming of resistance memory switches is an electro-reduction and drift process triggered by high electric field and enhanced by electrical heating [10]. One major issue in developing nanoscale switching devices is that devices based on metal oxides as the switching material are always needed an electroforming process to achieve the normal switching cycles. The electroforming process is typically done by applying a voltage sweep to a relatively high voltage to produce a significant change of the electronic conductivity of the device. The electroforming process is not a very well controlled operation and is potentially destructive, as the conductivity change is very sudden, and the voltage at which the change occurs varies from device-to-device [2]. Consequently, it is valuable to investigate the mechanism of the electroforming-free RS behavior and its relationship to the microstructure of RS materials.

Rare-earth (RE) metal oxides, including CeO_x, Gd_2O_3, and Lu_2O_3 [11], [12], are promising high-κ gate insulators in advanced complementary metal-oxide semiconductor (CMOS) devices because of their high resistivity, large dielectric constants, wide bandgaps, and good thermodynamic stability. These oxides were also investigated as a reversible RS material for resistance random access memory (RRAM) device applications [13]–[15]. However, CeO_x and Gd_2O_3 films are unstable in contact with the air and/or water because their lattice energies are small. Among RE_2O_3 oxides, Tm_2O_3, Yb_2O_3, and Lu_2O_3 are expected to be stable in contact with Si up to high temperatures during CMOS device fabrication processes due to their higher lattice energies and smaller ionic radii [16], [17]. Although the RE Gd_2O_3 thin film exhibited RS behavior free from the electroforming process [14], the deposition of this film is required for high-temperature processing. However, the electroforming-free RS behavior in Tm_2O_3, Yb_2O_3, and Lu_2O_3 thin materials has not been studied to date. In this paper, the electroforming-free RS characteristics in Ru/RE_2O_3/TaN (RE = Tm, Yb, and Lu) RRAM devices with full room temperature process were studied. The chemical structure of RE_2O_3 films was checked by X-ray photoelectron spectroscopy (XPS). The conduction mechanisms in both low-resistance state (LRS) and high-resistance state (HRS) of electroforming-free the Ru/RE_2O_3/TaN memory structures using Tm_2O_3, Yb_2O_3, and Lu_2O_3 thin films are discussed. Furthermore, the electrical characteristics in terms of data retention and endurance are shown for the Ru/RE_2O_3/TaN RRAM devices.

II. Experimental Procedure

The Ru/RE_2O_3/TaN RRAM devices were prepared through the following processes. After thermal oxidation of 4-in p-type (1 0 0) silicon wafers, a 50 nm-thick TaN layer was deposited as a bottom electrode by reactive sputtering. Then, a $\sim$20 nm-thick RE_2O_3 (Tm_2O_3, Yb_2O_3, or Lu_2O_3) thin film was deposited on TaN film at room temperature through radio frequency (rf) sputtering with a mixture of Ar and O_2 (Ar/O_2 = 3/1) from a

Manuscript received December 27, 2011; revised May 29, 2012; accepted July 10, 2012. Date of current version September 1, 2012. This work was supported in part by the National Science Council of Taiwan under Contract NSC-98-2221-E-182-056-MY3. The review of this paper was arranged by Associate Editor E. T. Yu.

T.-M. Pan, C.-H. Lu, and S. Mondal are with the Department of Electronics Engineering, Chang Gung University, Taoyuan 333, Taiwan (e-mail: tmpan@mail.cgu.edu.tw).

F.-H. Ko is with the Department of Materials Science and Engineering, Institute of Biological Science and Technology, National Chiao-Tung University, Hsinchu 300, Taiwan.

Color versions of one or more of the figures in this paper are available online at http://ieeexplore.ieee.org.

Digital Object Identifier 10.1109/TNANO.2012.2211893

1536-125X/$31.00 © 2012 IEEE

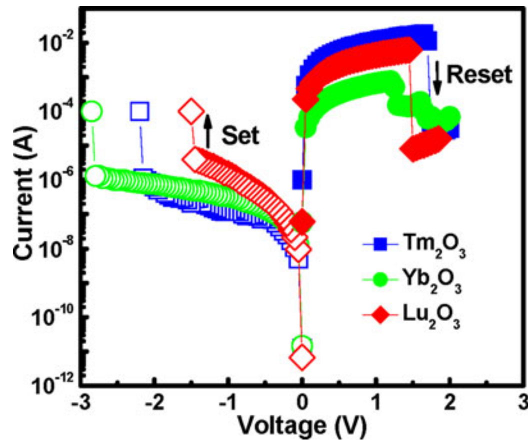

Fig. 1. Type *I*–*V* curves of resistive switching behavior in the Ru/RE_2O_3/TaN RRAM devices using Tm_2O_3, Yb_2O_3, and Lu_2O_3 thin films.

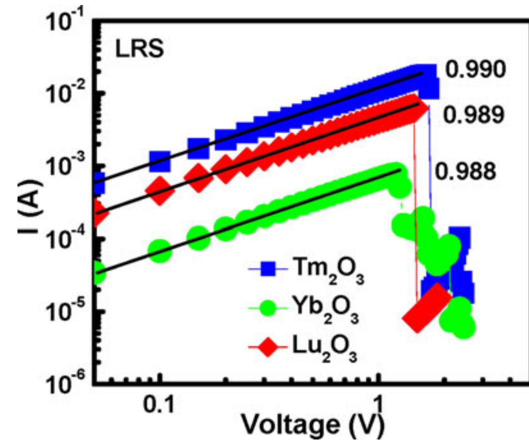

Fig. 2. Conducting mechanisms of Ru/RE_2O_3/TaN devices using Tm_2O_3, Yb_2O_3, and Lu_2O_3 films at LRS.

thulium, ytterbium, or lutetium target. The sputtering condition was a rf power of 100 W, process pressure of 10^{-3} torr, and base pressure of 1×10^{-6} torr. For electrical measurement, Ru top electrodes with a diameter of 200 μm were deposited by dc sputtering with a metal shadow mask. All processing step of Ru/RE_2O_3/TaN RRAM device was made in room temperature.

The composition and chemical bonding in each RE_2O_3 film were analyzed using a Thermo VG Scientific Microlab 350 system with a monochromatic Al K_α (1486.7 eV) source. The surface of the RE_2O_3 film was presputtered using an Ar ion source, operated at 5 kV for 3 min. The chemical shift in the spectra was corrected using the C ls peak from adventitious carbon at a binding energy of 285 eV. The curve-fit analyses after Shirley background subtraction were performed for Tm 4d, Yb 4d, Lu 4d, and O 1s photopeaks using Lorentzian–Gaussian functions to identify the functionalities associated with each element. All the current–voltage (*I*–*V*) characteristics of the fabricated devices were measured by an Agilent 4156 C semiconductor parameter analyzer using a dc voltage sweeping mode, in which the positive bias was defined by a current flow from Ru top electrode to TaN bottom electrode and the negative bias was defined by the opposite direction.

III. Results and Discussion

Fig. 1 shows comparisons of typical *I*–*V* characteristics of the Ru/RE_2O_3/TaN RRAM devices using Tm_2O_3, Yb_2O_3, and Lu_2O_3 thin films. Bipolar switching behaviors without electroforming process are observed on these Ru/RE_2O_3/TaN devices. By sweeping the voltage bias from zero to negative values, the current begins to increase gradually at a set voltage $V_{\rm set}$ and finally reaches a LRS. The compliance current was limited to 100 μA during sweeping voltage. Moreover, the current decreases suddenly at a reset voltage $V_{\rm reset}$ to return a HRS while sweeping the voltage bias from zero to positive values. The set process (change from HRS to LRS) occurs only under negative voltage bias and the reset process (change from LRS to HRS) only occurs under positive voltage bias. The LRS resistance for Tm_2O_3, Yb_2O_3, and Lu_2O_3 thin films is about 80, 1500, and 220 Ω, whereas HRS resistance is approximate 4.6, 1.2, and 2.2 MΩ, respectively. The Ru/Tm_2O_3/TaN and Ru/Lu_2O_3/TaN structure devices exhibited a higher resistance ratio of $\sim10^4$ than the Ru/Yb_2O_3/TaN device, suggesting the low density of metallic defects in the Yb_2O_3 film.

The current conduction in LRS is controlled by the ohmic transport at the TaN/RE_2O_3 interface. The curve of the log(*I*) versus log(*V*) for the Ru/RE_2O_3/TaN RRAM devices is a linear line with a slope of approximately 1, as shown in Fig. 2. The weak temperature dependence of the *I*–*V* curves in LRS also confirms the nearly ohmic conduction in the Ru/RE_2O_3/TaN device. In Fig. 3(a)–(c), the temperature-dependent log(*I*)–log(*V*) curves of the LRS samples using Tm_2O_3, Yb_2O_3, and Lu_2O_3 thin films, respectively, are shown. The *I*–*V* results for the Ru/RE_2O_3/TaN devices using Tm_2O_3, Yb_2O_3, and Lu_2O_3 thin films are plotted in the Ln(*I*) versus 1000/*T* form at the given voltages as shown in Fig. 3(d)–(f), respectively. From the slopes of the fitted lines, the activation energy E_a was calculated at each voltage. Fig. 4 depicts the variation in calculated E_a values of LRS and HRS as a function of the voltage for Ru/RE_2O_3/TaN memory devices. Each plot shows a generally straight line. The E_a value of LRS was determined to be about 0.02–0.03 eV, which are comparable to the thermal energy at room temperature.

The current conduction of the Tm_2O_3 resistive memory in HRS is governed by the space charge limited conduction (SCLC) [18]. The *I*–*V* fitting is shown in Fig. 5(a), in which three regions can be discriminated, denoted by I, II, and III, corresponding to ohmic emission, trap-filled-limit (TFL), and trap-free square-law, respectively. In region I, when the electric field across the RRAM device is small and the number of the thermally generated free electrons exceeds the injected electrons by the electric field, the current depends on the electric field and the material conductivity. The *I*–*V* curve follows Ohm's law and the slope of log(*I*) versus log(*V*) is almost equal to one. In region II, the injected electrons increase as the electric field increases. These injected electrons are partly trapped in the Tm_2O_3, i.e., injected trapped electrons; others donate to the total current, i.e., injected free electrons. This region is recognized as the charge injection limited and trap filling region. The existence of trapping centers in the Tm_2O_3 is fully occupied by injected

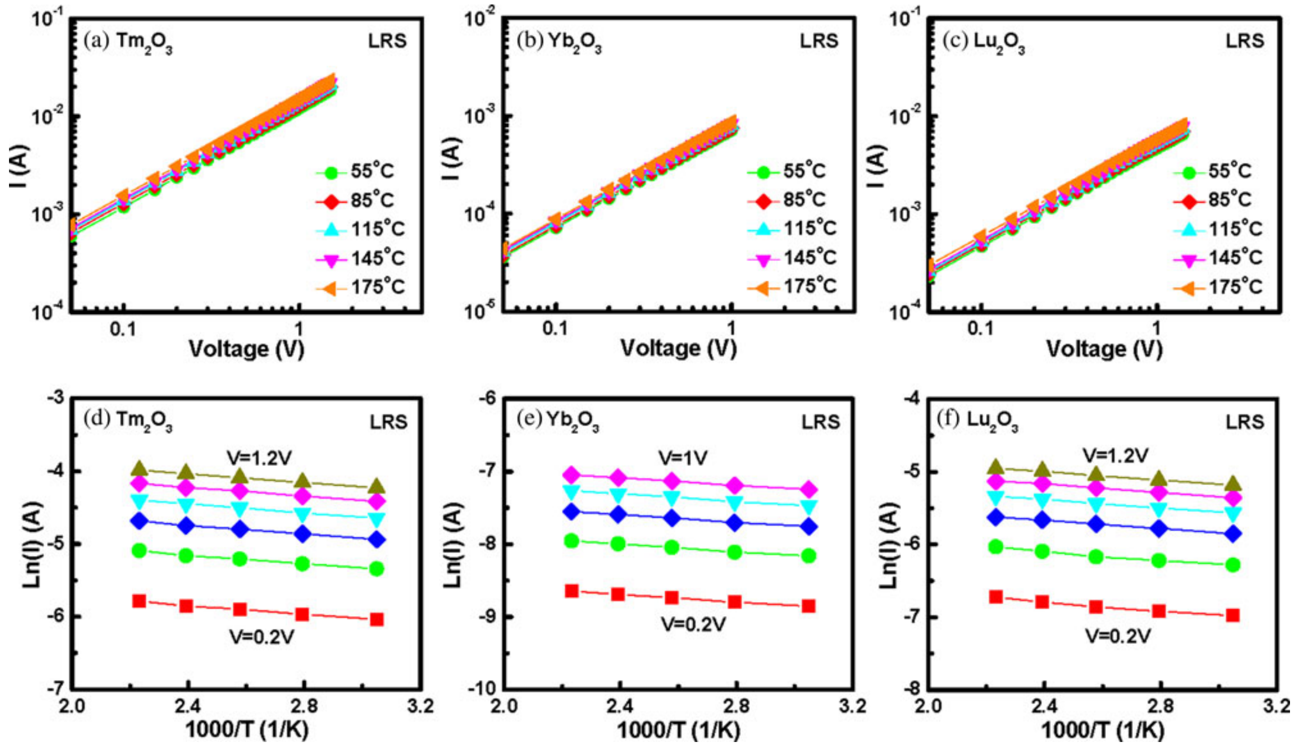

Fig. 3. Log(I)–log(V) curves of the (a) Tm_2O_3, (b) Yb_2O_3, and (c) Lu_2O_3 memory devices in LRS, measured at different temperatures. The Ln(I) versus 1000/T curves of the (d) Tm_2O_3, (e) Yb_2O_3, and (f) Lu_2O_3 memory devices in LRS at the given voltages.

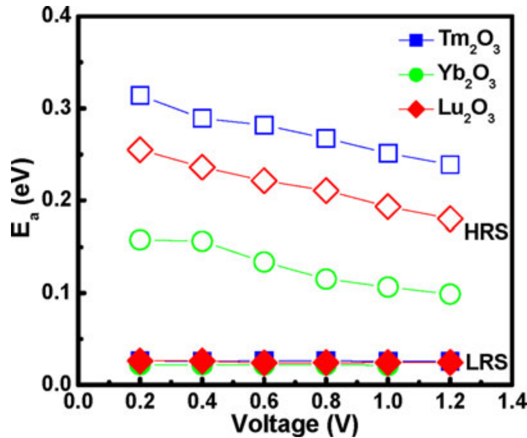

Fig. 4. Activation energy as a function of voltage for Ru/RE_2O_3/TaN RRAM devices at both LRS and HRS.

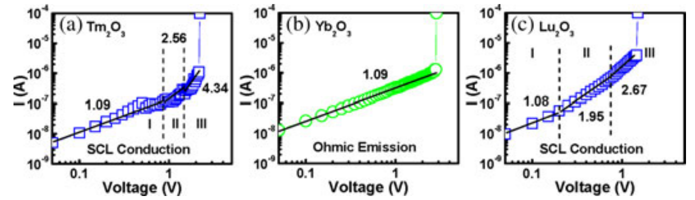

Fig. 5. The conducting mechanisms of (a) Tm_2O_3, (b) Yb_2O_3, and (c) Lu_2O_3 memory devices at HRS.

charge carriers, the current enters into region III. In this region, if the applied voltage increased further, more electrons will be injected from the Ru electrode that the Tm_2O_3 material cannot provide the excess electrons, and thereby the space charge begins to produce near the injecting electrode interface. In Fig. 5(b), the HRS current in the Yb_2O_3 resistive memory device is believed to be dominated by the ohmic behavior due to a slope of about 1 in the log(I) versus log(V) curve. In addition, the conduction mechanism of Ru/Lu_2O_3/TaN device in HRS fitted well to the SCLC mechanism, as shown in Fig. 5(c). The Lu_2O_3 film at the HRS exhibited a trap-controlled SCLC mechanism, including three distinct regions with different slopes, which correspond to the Ohm's law region, the TFL region from –0.2 to –0.75 V, and the trap-free square-law region above –0.75 V.

Fig. 6(a)–(c) shows the log(I)–log(V) curves of the Ru/RE_2O_3/TaN memory devices using Tm_2O_3, Yb_2O_3, and Lu_2O_3 thin films in the HRS, respectively, measured at various temperatures. The resistances in the Ru/RE_2O_3/TaN memory devices decreased as the temperature increased. The HRS shows a semiconducting (or oxide) behavior in the Ru/Tm_2O_3/TaN and Ru/Lu_2O_3/TaN memory devices, while the weak temperature dependency in the Ru/Yb_2O_3/TaN device confirms the ohmic-like conduction, corroborated well with earlier results. For the near-zero voltage region (0 to –0.15 V) in HRS, the carrier concentration is not affected by the weak carrier injection and ohmic conduction is observed. As the voltage increases in HRS, the I–V curves deviate from linear ohmic behavior due to the larger current injection. Fig. 6(d)–(f) demonstrates the Ln(I) of the Tm_2O_3, Yb_2O_3, and Lu_2O_3 thin films in the HRS plotted as a function of 1000/T, respectively. From the slopes of the fitted lines, the activation energy in the HRS was determined.

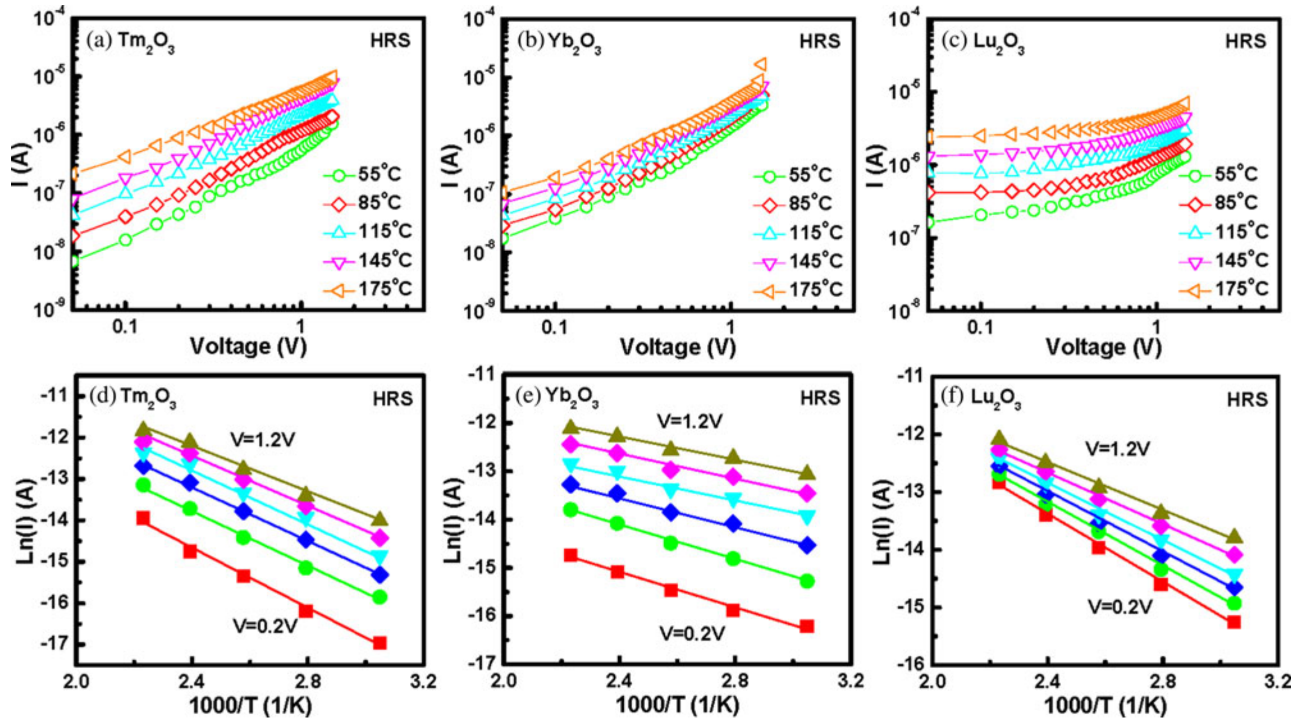

Fig. 6. Log(*I*)–log(*V*) curves of the (a) Tm_2O_3, (b) Yb_2O_3, and (c) Lu_2O_3 memory devices in HRS, measured at different temperatures. The Ln(*I*) versus 1000/*T* curves of the (d) Tm_2O_3, (e) Yb_2O_3, and (f) Lu_2O_3 memory devices in HRS at the given voltages.

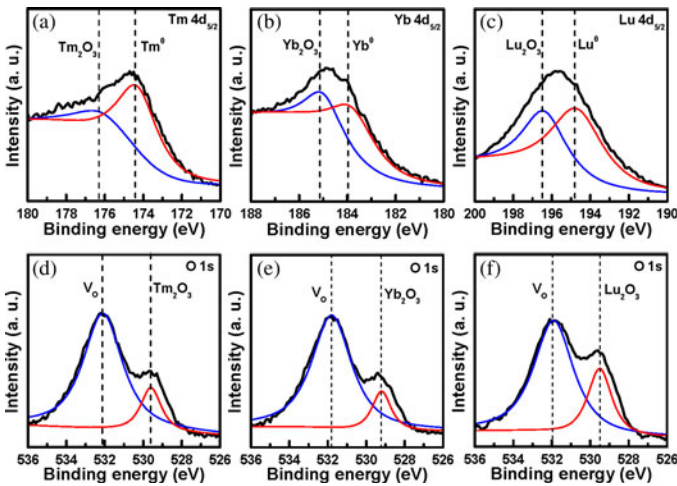

Fig. 7. (a) Tm 4d, (b) Yb 4d, (c) Lu 4d, and (d)–(e) O 1s XPS spectra of RE_2O_3 thin films deposited on $TaN/SiO_2/Si$.

The voltage dependence E_a values of $Ru/RE_2O_3/TaN$ memory devices are shown in Fig. 4. The E_a values for Tm_2O_3, Yb_2O_3, and Lu_2O_3 thin films were about 0.27, 0.13, and 0.22 eV, respectively. It is found that the Yb_2O_3 film has a lower E_a value than other films. This may be due to the specific property of this film and ohmic emission.

In order to realize the effect of the chemical defects in the RE_2O_3 film, the chemical states of RE and oxygen were explored by XPS. Fig. 7(a)–(c) present the Tm, Yb, and Lu $4d_{5/2}$ XPS spectra of the Tm_2O_3, Yb_2O_3, and Lu_2O_3 films, respectively. We assigned the Tm $4d_{5/2}$ peak at 176.2 and 174.3 eV to the thulium ion and metallic Tm^0 in Tm_2O_3, the Yb $4d_{5/2}$ peak at 185 and 183.8 eV to the ytterbium ion and metallic Yb^0 in Yb_2O_3, and the Lu $4d_{5/2}$ peak at 196.4 and 194.7 eV to the lutetium ion and metallic Lu^0 in Lu_2O_3 [17], respectively. The peak intensity of metallic Tm^0 in the Tm_2O_3 is higher than that of thulium ion, but the Yb_2O_3 film is inverse. Fig. 7(d) and (e) display the O atom binding energy of the XPS spectra of the Tm_2O_3, Yb_2O_3, and Lu_2O_3 films. Each of the RE_2O_3 films, the O 1s signal comprised two peaks: the lattice oxygen ion at 529.6 eV and the nonlattice oxygen ion at 532.1 eV in Tm_2O_3, the lattice oxygen ion at 529.2 eV and the nonlattice oxygen ions at 531.8 eV in Yb_2O_3, and the lattice oxygen ions at 529.5 eV and the nonlattice oxygen ions O at 531.9 eV in Lu_2O_3 [19], [20]. For the Lu_2O_3 film, the peak intensity of the O 1s peak corresponding to lattice oxygen ion showed higher compared with other films. The nonlattice oxygen ions were associated with $O_2{}^-$ ions in oxygen-deficient regions of RE_2O_3 films [14]. The nonlattice oxygen ion can work as the mobile oxygen. The interreactions between mobile oxygen and oxygen vacancies may give a clue for the generation of hysteresis and RS behavior [21].

The reason for the electroforming-free RS behavior in the $Ru/RE_2O_3/TaN$ structure is investigated, while the electroforming process is usually needed to form the conducting filaments for other binary transition oxides. The mechanism of unipolar RS behavior in the Nd_2O_3, Dy_2O_3, and Er_2O_3 film materials has been demonstrated in our previous studies [22]. The generation of metallic atoms and nonlattice oxygen ions play a critical role in RS behavior free from electroforming process. During the deposition process, a high number of crystal defects preexisting in the RE_2O_3 film could contribute to the formation of the conducting paths without the forming process. If the number

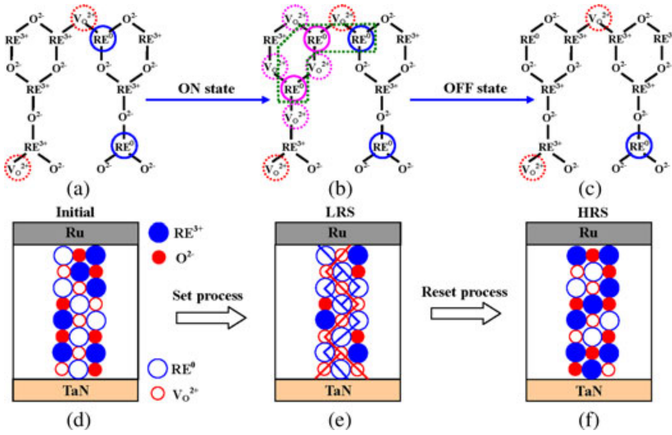

Fig. 8. Schematic diagram of resistance switching mechanism in RE_2O_3 thin films for (a) conduction, (b) formation of filament, (c) rupture of filament, (d) initial, (e) LRS, and (f) HRS.

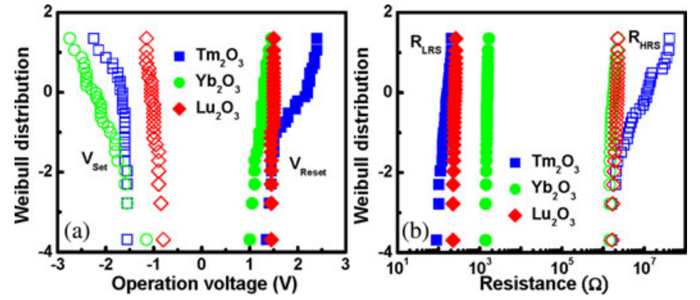

Fig. 9. Weibull distributions of the (a) $V_{\rm set}$ and $V_{\rm reset}$, as well as (b) $R_{\rm LRS}$ and $R_{\rm HRS}$ for Ru/RE_2O_3/TaN RRAM devices prepared with Tm_2O_3, Yb_2O_3, and Lu_2O_3 films.

of chemical defects may exceed the percolation threshold, the RE_2O_3 film becomes a conductive layer with low resistance. The generation of conductive filaments should be attributed to the localized agglomeration of the oxygen vacancies in RE_2O_3 film [23], as shown in Fig. 8(a). Fig. 8(d) illustrates that the presence of conduction paths consist of metallic RE and oxygen vacancies in the RE_2O_3 film. According to the model of formation and rupture of a conductive filament [24], we described a microscopic view for the RS in Ru/RE_2O_3/TaN device. Formation and rupture of a conductive filament is due to a redox reaction in the oxide film under a voltage bias. The chemical equation in Kröger–Vink notation for the formation of one oxygen vacancy is as follows:

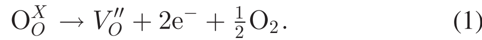

$$\mathrm{O}_O^X \rightarrow V_O'' + 2\mathrm{e}^- + \tfrac{1}{2}\mathrm{O}_2. \quad (1)$$

The oxygen ions incorporating in RE-O bonds may migrate resulting in +2 oxygen vacancy, stable charge state, and two electrons to be localized on the nearby RE atoms [see Fig. 8(a)]. They tend to cluster connections in certain configurations with lower V_o–V_o interactions [25]. Considering a RE atom in the vicinity of these oxygen vacancies the charge state of this RE atom may become $RE_2{}^+$, RE^+, or RE^0 as follows:

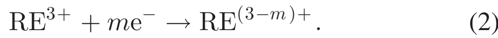

$$\mathrm{RE}^{3+} + m\mathrm{e}^- \rightarrow \mathrm{RE}^{(3-m)+}. \quad (2)$$

The oxygen vacancies migrate toward the cathode when a voltage bias is applied to a switching material. In this case, the dominant driving force for migration is the gradient of electrostatic potential applied through the oxide film. Therefore, the formation of the conduction filament is due to oxygen ions migration between two electrodes by creating a large number of oxygen vacancies and metallic RE atoms within the oxide thin films. The oxygen vacancies and metallic RE atoms are connected in a chain, as shown in Fig. 8(b). Fig. 8(e) depicts that the conduction of LRS is due to electron hopping transport among localized oxygen vacancies and metallic RE atoms in the conductive filament paths. Thus, the chain can be regarded as a conduction filament representing the "Set" state. After the "Set" process, if a positive voltage bias is applied, the current density through a conduction filament reaches high values and might be responsible for producing the thermal energy. The high temperature due to Joule heating will activate the migration of oxygen at the highest resistive point or at the electrode-filament interface [26]. In addition, the high concentration of oxygen vacancy (positive charged) can enhance its capture cross section to nonlattice oxygen ions (negative charged) and, hence, the recover probability of oxygen vacancy with nonlattice oxygen ions increases. Consequently, the rupture process of the conduction filament is due to oxygen migration back to oxygen vacancy sites in the filamentary path and oxidation of those RE atoms to recover their RE–O bonds in bulk like oxygen coordination, as shown in Fig. 8(c). The annihilation of oxygen vacancies and recovery of metallic RE atoms can be regarded as the rupture of filament indicating the "Reset" state, as shown in Fig. 8(f). Notably, a stable RS behavior can be achieved for negative set and positive reset processes only. For a negative set process, the oxygen ions are migrated to the Ru electrode by producing defects in the oxide to form a metallic filamentary path and the device switches from HRS to LRS. The migrated oxygen ions are adsorbed at the Ru electrode and a metallic stable RuO_x layer formed by the oxidation at the Ru/oxide interface. During the reset process by opposite polarity of bias, the rupture of filament by the annihilation of oxide defects become difficult due to the irreversible oxidation of a metallic Ru electrode.

Fig. 9(a) and (b) depicts the Weibull distributions of the $V_{\rm set}$, $V_{\rm reset}$, $R_{\rm LRS}$, and $R_{\rm HRS}$ for the Ru/RE_2O_3/TaN devices. The distribution of the Ru/Lu_2O_3/TaN memory device showed a lower set voltage than other devices, suggesting the high concentration of the lutetium ions in Lu_2O_3 leading to more conductive path. Moreover, the intrinsic high energy of the 5d shell and its low occupancy (only one electron for Lu) should limit the density of chemical defects in Lu_2O_3 film [27]. The distribution ranges of $V_{\rm set}$, $V_{\rm reset}$, $R_{\rm LRS}$, and $R_{\rm HRS}$ of Ru/Lu_2O_3/TaN memory devices are from –0.8 to –1.15 V, 1.45 to 1.5 V, 210 to 260 Ω, and 1.65 to 2.31 MΩ, respectively. Although $V_{\rm set}$, $V_{\rm reset}$, $R_{\rm LRS}$, and $R_{\rm HRS}$ of this device are fluctuating, they are below 30%. The Ru/Yb_2O_3/TaN device has a high LRS resistance due to the low content of chemical defects such as oxygen vacancies, metallic defects, and dislocations in the Yb_2O_3 thin film. The ytterbium can easily produce a structural defect due to a critical mixed-valence material [28], resulting in ohmic conduction in the HRS and LRS. Although the $R_{\rm HRS}$ distribution of the

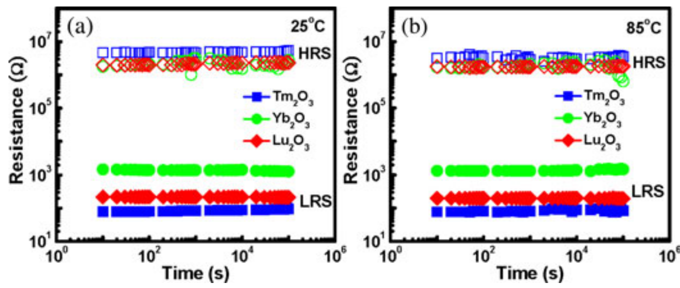

Fig. 10. Retention characteristics of both resistance states for Ru/RE_2O_3/TaN devices under a continuous ±0.5 V readout voltage, measured at (a) 25 °C and (b) 85 °C.

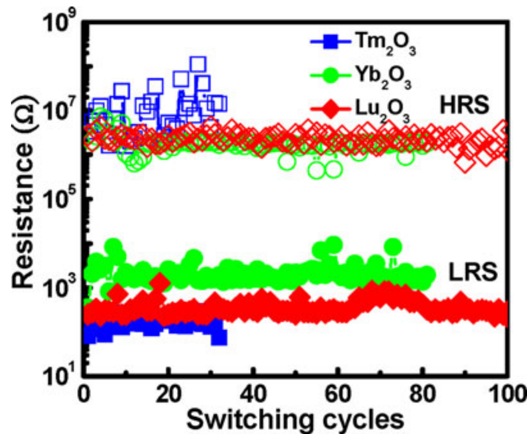

Fig. 11. Resistance values of both HRS and LRS versus cycle numbers for Ru/RE_2O_3/TaN RRAM devices using Tm_2O_3, Yb_2O_3, and Lu_2O_3 films.

Ru/Tm_2O_3/TaN device had a high resistance, it also exhibited a nonuniformity of the resistance distribution. This phenomenon could be attributed to the creation of a large number of conductive filament paths.

Fig. 10(a) and (b) illustrates the retention of the Ru/RE_2O_3/TaN memory devices using Tm_2O_3, Yb_2O_3, and Lu_2O_3 thin films under ±0.5 V reading voltage at 25 and 85 °C, respectively. Both LRS and HRS resistances, the Tm_2O_3 and Lu_2O_3 films measured at 25 °C are stable with no obvious degradation for 10^5 s, indicating that these devices exhibited nondestructive readout and good reliability. These films may be attributed to sufficient barriers to inhibit the escape of the trapped electronic charge by thermally activated or tunneling processes. The Yb_2O_3 memory devices tested at 25 and 85 °C degraded more quickly at –0.5 sampling voltage than that at 0.5 sampling voltage. It is probable that negative voltage accelerate the oxygen ion diffusion rate from Ru electrode to Yb_2O_3 film that causes the recombination of nonlattice oxygen ion and oxygen vacancy.

The endurance characteristics of the Ru/RE_2O_3/TaN RRAM devices using Tm_2O_3, Yb_2O_3, and Lu_2O_3 thin films are shown in Fig. 11. The resistance ratio of the Ru/Lu_2O_3/TaN device between two states is about 10^4 after 100 switching cycles. However, the RS behavior in Tm_2O_3 film exhibited the unstable switching cycle less than 40. This unstable RS may be due to insufficient nonlattice oxygen ions to recover the oxygen vacancies under a reset voltage. The better RS performance of the Ru/Lu_2O_3/TaN structure memory, compared with the Al/CuO_x/Cu [29], Pt/SnO_2/Pt [30], and Ti/TiO_2/Pt [31] structures fabricated at room temperature, is in terms of higher resistance ratio and better data retention. Although Ru/Lu_2O_3/TaN structure has a slightly larger set and reset voltage, the thickness of the Lu_2O_3 film can be reduced to achieve a lower set and reset voltage.

IV. Conclusion

The electroforming-free RS characteristics of RE_2O_3-based RRAM devices with full room temperature process have been demonstrated. The conduction mechanism of low-resistance state for Ru/RE_2O_3/TaN memory devices is ohmic emission, while high-resistance state for Tm_2O_3, Yb_2O_3, and Lu_2O_3 memory devices is SCLC, ohmic behavior, and SCLC, respectively. The metallic RE and nonlattice oxygen ion were obtained based on XPS analyses. This Ru/Lu_2O_3/TaN memory device exhibited good electrical characteristics in terms of resistance ratio, device yield, data retention, and endurance, presumably due to the optimal content of chemical defects, such as metallic Lu and nonlattice oxygen ion, in Lu_2O_3 film. The electroforming-free switching mechanism of the Ru/RE_2O_3/TaN RRAM devices could be explained using well-established filamentary theory. The Ru/Lu_2O_3/TaN memory device should have attracted much attention for next-generation nonvolatile memory applications.

References

[1] G. I. Meijer, "Who wins the nonvolatile memory race?" *Science*, vol. 319, no. 4, pp. 1625–1626, Mar. 2008.
[2] D. S. Jeong, H. Schroeder, U. Breuer, and R. Waser, "Characteristic electroforming behavior in Pt/TiO_2/Pt resistive switching cells depending on atmosphere," *J. Appl. Phys.*, vol. 104, no. 12, pp. 123716-1–123716-8, Dec. 2008.
[3] S. Seo, M. J. Lee, D. H. Seo, E. J. Jeoung, D. S. Suh, Y. S. Joung, I. K. Yoo, I. R. Hwang, S. H. Kim, I. S. Byun, J. S. Kim, J. S. Choi, and B. H. Park, "Reproducible resistance switching in polycrystalline NiO films," *Appl. Phys. Lett.*, vol. 85, no. 23, pp. 5655–5657, Dec. 2008.
[4] S. O. Kang, S. Hong, J. Choi, J. S. Kim, I. Hwang, I. S. Byun, K. S. Yun, and B. H. Park, "Electrochemical growth and resistive switching of flat-surfaced and (1 1 1)-oriented Cu_2O films," *Appl. Phys. Lett.*, vol. 95, no. 9, pp. 092108-1–092108-3, Sep. 2009.
[5] W. C. Chien, Y. C. Chen, E. K. Lai, Y. D. Yao, P. Lin, S. F. Horng, J. Gong, T. H. Chou, H. M. Lin, M. N. Chang, Y. H. Shih, K. Y. Hsieh, R. Liu, and C. Y. Lu, "Unipolar switching behaviors of RTO WO_X RRAM," *IEEE Electron Device Lett.*, vol. 31, no. 2, pp. 126–128, Feb. 2010.
[6] K. M. Kim, B. J. Choi, B. W. Koo, S. Choi, D. S. Jeong, and C. S. Hwang, "Resistive switching in Pt/Al_2O_3/TiO_2/Ru stacked structures," *Electrochem. Solid-State Lett.*, vol. 9, no. 12, pp. G343–G346, Dec. 2006.
[7] E. A. Miranda, C. Walczyk, C. Wenger, and T. Schroeder, "Model for the resistive switching effect in HfO_2 MIM structures based on the transmission properties of narrow constrictions," *IEEE Electron Device Lett.*, vol. 31, no. 6, pp. 609–611, Jun. 2010.
[8] Q. Zuo, S. Long, S. Yang, Q. Liu, L. Shao, Q. Wang, S. Zhang, Y. Li, Y. Wang, and M. Liu, "ZrO_2-based memory cell with a self-rectifying effect for crossbar WORM memory application," *IEEE Electron Device Lett.*, vol. 31, no. 4, pp. 344–346, Apr. 2010.
[9] W. Y. Chang, C. A. Lin, J. H. He, and T. B. Wu, "Resistive switching behaviors of ZnO nanorod layers," *Appl. Phys. Lett.*, vol. 96, no. 24, pp. 242109-1–242109-3, Jun. 2010.
[10] J. J. Yang, F. Miao, M. D. Pickett, D. A. A. Ohlberg, D. R. Stewart, C. N. Lau, and R. S. Williams, "The mechanism of electroforming of metal

oxide memristive switches," *Nanotechnology*, vol. 20, no. 21, pp. 215201-1–215201-9, May 2009.

[11] O. Engstrom, B. Raeissi, S. Hall, O. Buiu, M. C. Lemme, H. D. B. Gottlob, P. K. Hurley, and K. Cherkaoui, "Navigation aids in the search for future high-k dielectrics: Physical and electrical trends," *Solid-State Electron.*, vol. 51, no. 4, pp. 622–626, 2007.

[12] M. Fanciulli and G. Scarel, *Rare Earth Oxide Thin Film: Growth, Characterization, and Applications*. Berlin, Germany: Springer, 2007.

[13] X. Sun, B. Sun, L. Liu, N. Xu, X. Liu, R. Han, J. Kang, G. Xiong, and T. P. Ma, "Resistive switching in CeO_x films for nonvolatile memory application," *IEEE Electron Device Lett.*, vol. 30, no. 4, pp. 334–336, Apr. 2009.

[14] X. Cao, X. Li, X. Gao, W. Yu, X. Liu, Y. Zhang, L. Chen, and X. Cheng, "Forming-free colossal resistive switching effect in rare-earth-oxide Gd_2O_3 films for memristor applications," *J. Appl. Phys.*, vol. 106, no. 7, pp. 073723-1–073723-5, Oct. 2009.

[15] X. Gao, Y. Xia, B. Xu, J. Kong, H. Guo, K. Li, H. Li, H. Xu, K. Chen, J. Yin, and Z. Liu, "Unipolar resistive switching behaviors in amorphous lutetium oxide films," *J. Appl. Phys.*, vol. 108, no. 7, pp. 074506-1–074506-5, Oct. 2010.

[16] S. Ohmi, C. Kobayashi, I. Kashiwagi, C. Ohshima, H. Ishiwara, and H. Iwai, "Characterization of La_2O_3 and Yb_2O_3 thin films for high-*k* gate insulator application," *J. Electrochem. Soc.*, vol. 150, no. 6, pp. F134–F140, Jun. 2003.

[17] H. Ono and T. Katsumata, "Interfacial reactions between thin rare-earth-metal oxide films and Si substrates," *Appl. Phys. Lett.*, vol. 78, no. 13, pp. 1832–1834, Mar. 2001.

[18] F. C. Chiu, H. W. Chou, and J. Y. Lee, "Electrical conduction mechanisms of metal/La_2O_3/Si structure," *J. Appl. Phys.*, vol. 97, no. 10, pp. 103503-1–103503-5, 2005.

[19] Y. A. Teterin and A. Y. Teterin, "Structure of X-ray photoelectron spectra of lanthanide compounds," *Russian Chem. Rev.*, vol. 71, no. 5, pp. 347–381, 2002.

[20] J. F. Moulder, W. F. Stickle, P. E. Sobol, and K. D. Bomben, *Handbook of X-Ray Photoelectron Spectroscopy: A Reference Book of Standard Spectra for Identification and Interpretation of XPS Data*. Chanhassen, MN: Physical Electronics, Inc., 1995.

[21] R. Dong, W. F. Xiang, D. S. Lee, S. J. Oh, D. J. Seong, S. H. Heo, H. J. Choi, M J. Kwon, M. Chang, M. Jo, M. Hasan, and H. Hwang, "Improvement of reproducible hysteresis and resistive switching in metal-$La_{0.7}Ca_{0.3}MnO_3$-metal heterostructures by oxygen annealing," *Appl. Phys. Lett.*, vol. 90, no. 18, pp. 182118-1–182118-3, May 2007.

[22] T. M. Pan and C. H. Lu, "Forming-free resistive switching behavior in Nd_2O_3, Dy_2O_3, and Er_2O_3 films fabricated in full room temperature," *Appl. Phys. Lett.*, vol. 99, no. 11, pp. 113509-1–113509-3, Sep. 2011.

[23] L. Nagarajan, R. A. De Souza, D. Samuelis, I. Valov, A. Borger, J. Janek, K. D. Becker, P. C. Schmidt, and M. Martin, "A chemically driven insulator–metal transition in non-stoichiometric and amorphous gallium oxide," *Nature Mater.*, vol. 7, no. 5, pp. 391–398, May 2008.

[24] H. D. Lee, B. Magyari-Kope, and Y Nishi, "Model of metallic filament formation and rupture in NiO for unipolar switching," *Phys. Rev. B*, vol. 81, no. 19, pp. 193202-1–193202-4, May 2010.

[25] D. A. Muller, N. Nakagawa, A. Ohtomo, J. L. Grazul, and H. Y. Hwang, "Atomic-scale imaging of nanoengineered oxygen vacancy profiles in $SrTiO_3$," *Nature*, vol. 430, no. 7360, pp. 657–661, Aug. 2004.

[26] U. Russo, C. Cagli, S. Spiga, E. Cianci, and D. Ielmini, "Impact of electrode materials on resistive-switching memory programming," *IEEE Electron Device Lett.*, vol. 30, no. 8, pp. 817–819, Aug. 2009.

[27] G. Lucovsky, Y. Zhang, G. B. Rayner, G. Appel, H. Ade, and J. L. Whitten, "Electronic structure of high-k transition metal oxides and their silicate and aluminate alloys," *J. Vac. Sci. Technol. B*, vol. 20, no. 4, pp. 1739–1747, Jul. 2002.

[28] L. Marsella and V. Fiorentini, "Structure and stability of rare-earth and transition-metal oxides," *Phys. Rev. B*, vol. 69, no. 17, pp. 172103-1–172103-4, May 2004.

[29] H. Lv, H. Wan, and T. Tang, "Improvement of resistive switching uniformity by introducing a thin GST interface layer," *IEEE Electron Device Lett.*, vol. 31, no. 9, pp. 978–980, Sep. 2010.

[30] K. Nagashima, T. Yanagida, K. Oka, and T. Kawai, "Unipolar resistive switching characteristics of room temperature grown SnO_2 thin films," *Appl. Phys. Lett.*, vol. 94, no. 24, pp. 242902-1–242902-3, Jun. 2009.

[31] J. J. Huang, C. W. Kuo, W. C. Chang, and T. H. Hou, "Transition of stable rectification to resistive-switching in Ti/TiO_2/Pt oxide diode," *Appl. Phys. Lett.*, vol. 96, no. 26, pp. 262901-1–262901-3, Jun. 2010.

Tung-Ming Pan was born in Taipei, Taiwan, 1970. He received the B.S. degree from the Department of Electronics Engineering, National Chiao-Tung University (NCTU), Taiwan, in 1997, and the Ph.D. degree from the Institute of Electronics, NCTU, in 2001.

From 2000 to 2002, he joined the LOGIC Development Department, Technology and Process Development Division (TD), United Microelectronics Corporation (UMC), as a principal engineer. He was engaged in developing the 0.1 μm device and process. Then, he transferred to the Reliability Engineering, Quality and Reliability Assurance Division. He was responsible to the 0.1 μm device reliability and quality. In 2002, he jointed the mixed signal team of Elansat Tech. Corporation as a Senior Engineer. He was engaged to design high-speed analog-to-digital converter (ADC) and digital-to-analog converter (DAC). In 2004, he joined the faculty at Chang Gung University as an Assistant Professor in the Department of Electronics Engineering, and became a Professor in 2009. He has published more than 130 SCI journal papers, and is the author or coauthor of six patents. His current research interests include the high-κ gate dielectric materials, nonvolatile memories, thin-film transistors (TFTs), nano-CMOS devices and technologies, reliability of semiconductor devices, biosensor materials, and devices.

Chih-Hung Lu was born in Changhwa, Taiwan, on May 22, 1985. He received the B.S. degree in electronics engineering from Southern Taiwan University, Tainan, Taiwan, in 2008, and the M.S. degree in electronics engineering from Chang Gung University, Taoyuan, Taiwan, in 2010. He is currently working toward the Ph.D. degree in the Institute of Electronics, National Chiao-Tung University.

Somnath Mondal received the M.Sc. degree in electronic science from Jadavpur University, Kolkata, India, in 2005. He is currently working toward the Ph.D. degree at the Thin Film Measurement Laboratory, Graduate Institute of Electronic Engineering, Chang Gung University, Taoyuan, Taiwan.

His research interests include alternative high-κ material for CMOS gate dielectrics, metal–insulator–metal capacitor applications and resistive random access memory.

Fu-Hsiang Ko was born in Hsinchu, Taiwan, in 1965. He received the B.S. and M.S. degrees in chemistry from National Tsing Hua University, Hsinchu, Taiwan, and National Taiwan Normal University, Taipei, Taiwan, in 1989 and 1991, respectively, and the Ph.D. degree in atomic science from National Tsing Hua University in 1996.

He joined National Nano Device Laboratories, Hsinchu, as an Associate Researcher in 1996, and became a Researcher in 2002. He moved to Department of Materials Science and Engineering, National Chiao Tung University, as an Associate Professor and Full Professor in February 2005 and August 2007, respectively. He is currently engaged in developing the electron beam lithography, chemical treatment technologies, conventional silicon microelectronics, and new-style bottom-up devices (biosensors or molecular electronics).